Universiteit
Leiden
The Netherlands

On the Miniaturization of the Magnetic Paul Trap

Bent, Eli van der

Citation
Bent, E. van der. (2024). *On the Miniaturization of the Magnetic Paul Trap*.

Version:	Not Applicable (or Unknown)
License:	License to inclusion and publication of a Bachelor or Master Thesis, 2023
Downloaded from:	https://hdl.handle.net/1887/3736637

Note: To cite this publication please use the final published version (if applicable).

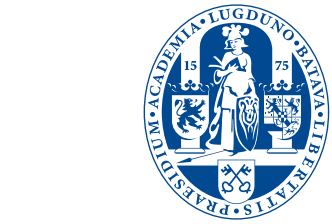

On the Miniaturization of the Magnetic Paul Trap

THESIS

submitted in partial fulfillment of the
requirements for the degree of

MASTER OF SCIENCE
in
PHYSICS

Author :	E.H.J. van der Bent
Student ID :	s1998617
Supervisor :	Dr.ir. B.J. Hensen
	Drs. M.A. Janse
2^{nd} corrector :	Dr. W. Löffler

Leiden, The Netherlands, March 1st, 2024

On the Miniaturization of the Magnetic Paul Trap

E.H.J. van der Bent

Huygens-Kamerlingh Onnes Laboratory, Leiden University
P.O. Box 9500, 2300 RA Leiden, The Netherlands

March 1st, 2024

Abstract

In this thesis we present an experimental realisation of a double loop type Magnetic Paul Trap. We show that a microgram heavy NdFeB permanent magnet can stably be levitated for hours at room temperature in this trap. Magnetic levitation of a magnetized particle is theoretically possible with this trap by generating opposed alternating magnetic fields. We show the fabrication of a printed circuit structure capable of producing these fields, as well as the engineering behind the realisation of the trap. Both by optical and magnetic readout we characterize the motion of the trapped magnet and show that its center of mass motion frequencies $\omega_z = 2\omega_{x,y} \approx 20Hz$. We characterize the damping on these modes and find that at low pressure the quality factor is strongly limited (to $Q \approx 90$) by coupling to the environment through generation of Eddy currents.

CONTENTS

1. INTRODUCTION

Bringing particles into a state of stable and controlled levitation is a field of considerable interest. Controlling the trapping of a particle disconnected from environmental inputs allows the building of experimental platforms to study atoms, microparticles, materials, quantum systems among others in more isolated regimes than other techniques provide. Levitation in a vacuum isolates a particle from direct physical contact with other materials, preventing unwanted coupling to external factors like heating and leaving its degrees of freedom to evolve and interact freely [1]. Optical, electric and magnetic techniques for trapping dielectric, charged and magnetized particles, each have advantages and drawbacks and consequently have varying applications regarding what type of particle is studied. Magnetic levitation stands out among the three as a method of trapping very large particles (μm to cm) in either cryogenic regimes with static fields making use of the Meissner effect, or at room temperature with rotating or otherwise changing fields [2]. The drawback of larger particles is their lower trapping frequency, significantly reducing the speed at which center-of-mass cooling can be done. Trapping heavier particles plays a crucial part in quantum research, where experimental resolve is looked at for guidance regarding quantum gravity theory [3]. Bringing levitated heavy particles ($\sim$ *picogram*) close to the quantum ground state through cooling has been proposed to measure the quantum nature of gravity through gravity mediated entanglement [4, 5]. Two heavy particles' entanglement would, being isolated from other entangling factors, be mostly dependent on the gravitational force between them, if the gravitational field can act as a quantum mediator. The larger the mass of these particles, the easier the entanglement would be to measure.

The project presented in this thesis is concerned with the proposal of magnetically levitating a large particle as discussed in [2]. There it is shown that a permanent magnet ($\sim$cm) can be stably levitated without the Meissner effect and despite Earnshaw's theorem (stating that levitation with static fields is impossible) through the use of a rotating, saddle-shaped magnetic field, which is coined the Magnetic Paul Trap (after its electric counterpart, the Paul Trap). It is further proposed that, based on

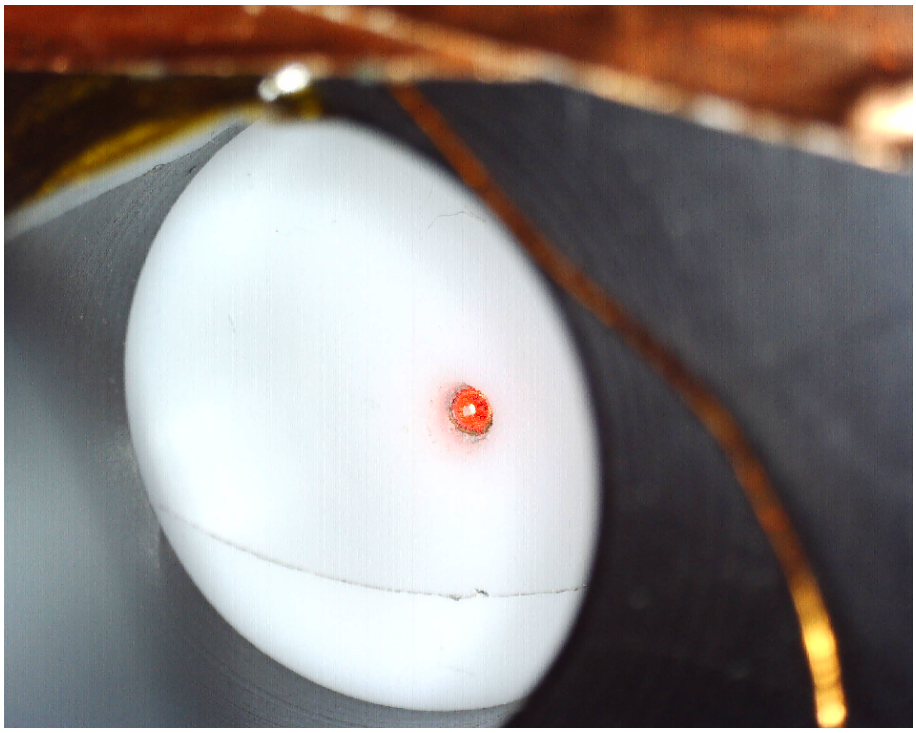

Figure 1.1: *The Magnetic Paul Trap in action. We see the black plastic of the top Helmholtz coil, and the inner white teflon as a spacer between the PCB, on which the trap structure is printed, and the glass cover keeping the magnet closed in. The red light (632.8nm) He-Ne laser, redirected with a mirror to point directly upward through the trap, is seen to illuminate the levitating cube magnet from the bottom. Some wiring and thermalising copper tape is seen in the top of the picture.*

their working principle, an on-chip trap with a double-loop design should also be able to levitate a magnetized particle ($\sim \mu$m). In the chapters that follow we show our successful realisation of this novel Magnetic Paul Trap with a PCB (Printed Circuit Board) design as well as our attempts at measuring and characterizing the motion of a NdFeB cube magnet (250μm).

2. THEORY

2.1 Levitodynamics

From the analytical expression for the magnetic field generated by the trap loops and the magnetic moment of the particle the magnetic energy of the particle can be approximated through a second-order Taylor expansion with $E_{mag} = -\boldsymbol{\mu} \cdot \boldsymbol{B}$. A dimensionless stability factor q is introduced Eq. 2.1 for which the secular approximation is valid when $q \leq 0.4$ which allows averaging over the field oscillations and obtaining the motional frequencies [2]:

$$q_z = -2q_x = -2q_y = \frac{2B_1^{''}B_{sat}}{\mu_0 \rho_m \Omega^2} \tag{2.1}$$

in which $B_1^{''}$ is the magnitude of the curvature of the trap-generated field, B_{sat} is the field strength of the magnetized particle at saturation, also called the remanent field. μ_0 is the magnetic permeability in vacuum, ρ_m the mass density of the material of the particle and Ω the radial trapping frequency. The frequencies of the center-of-mass modes in x, y and z, where the trap loops lie in the x, y–plane and z is the height, are given by Eq. 2.2.

$$\omega_z = 2\omega_x = 2\omega_y = \frac{\Omega}{2}\frac{|q_z|}{\sqrt{2}} \tag{2.2}$$

As long as the stability criterion is obeyed the equation can be written without q to see that the CoM eigenfrequencies are directly proportional and inversely proportional to the trap field curvature and the trap frequency respectively Eq. 2.3.

$$\omega_z = 2\omega_x = 2\omega_y = \frac{1}{\sqrt{2}}\frac{|B_1^{''}|B_{sat}}{\mu_0 \rho_m \Omega} \tag{2.3}$$

The librational frequencies ω_γ and ω_β, which are the rotations around the x and y axes, are given by Eq. 2.4 and depend on the strength of the

homogeneous aligning field, which makes sense as these modes are vibrations in the alignment of the particle along the z-axis.

$$\omega_\gamma = \omega_\beta = \sqrt{\frac{5}{2}\frac{B_0 B_{sat}}{\mu_0 \rho_m a^2}} \tag{2.4}$$

Here a is the radius of the particle. In the mathematical model the trap and magnet are rotationally invariant along the z-axis, which is why there is no mode associated with the particle rotating along this axis. However, we will call this rotation by the angle α.

The motion of the levitated particle does not directly depend on the the gradient $B_2^{'}$, but it does depend on the curvature $B_1^{''}$ which is not constant everywhere around the trap. The magnet is confined in the x- and y direction, but its equilibrium height can be controlled by changing the gradient. We can approximate the curvature's dependence on the height z above the trap and thus find an expected relation between $B_2^{'}$ and the CoM eigenfrequencies of the motion. The strength of a magnetic field of a coil with N windings, with radius R carrying a current I at a distance z from the center of the coil reads:

$$B(z) = \frac{\mu_0 N I R^2}{2(R^2 + z^2)^{\frac{3}{2}}} \tag{2.5}$$

The curvature of this field is found as:

$$B^{''}(z) = \frac{d^2 B(z)}{dz^2} = \frac{3}{2}\frac{\mu_0 I N R^2 \cdot \left(4z^2 - R^2\right)}{(z^2 + R^2)^{\frac{7}{2}}} \tag{2.6}$$

from which follows:

$$B_1^{''}(z) \underset{z>R}{\sim} \frac{1}{z^5} \tag{2.7a}$$

$$B_1^{''}(z) \underset{z\approx R}{\sim} \frac{1}{z} \tag{2.7b}$$

$$B_1^{''}(z) \underset{z<R}{\sim} \frac{1}{z^2} \tag{2.7c}$$

The force of a magnetic field on a permanent magnet with homogeneous magnetization can be calculated from:

$$\boldsymbol{F}_{mag} = -\mu \cdot \nabla \boldsymbol{B} \tag{2.8}$$

which results in the relation between the equilibrium height of a levitated particle and the gradient field $B_2{}'$:

$$z \sim \frac{F_{mag}}{m\omega_z^2} \sim B_2{}' \tag{2.9}$$

In conclusion, the linearity of the relationships between the current through our Helmholtz coils, the generated gradient between them and the displacement in height due to that gradient together with the linear relation between the CoM mode frequencies and the curvature of the trap fields can tell us in what region (Eqs. 2.7) above the trap our magnet is levitating.

2.2 Damping

As discussed our setup can be placed in a vacuum chamber. We wish to study the effect of depressurizing the environment of the levitated magnet to find how strongly its motion is gas-damped. Given the linear relationship between pressure and number of particles from the ideal gas law, we would expect an inverse relationship between the gas-damping dependent quality factor Q_{gas} and the pressure. The magnet dissipates energy to its environment by colliding with gas particles, therefore the damping depends on the number of particles. An inverse relation between the quality factor and the pressure has been suggested for levitated particles [6] as well as resonators [7]. The total quality factor is most likely not only dependent on the pressure. The magnet is of a conducting material, through which Eddy currents can be generated by the plethora of magnetic fields of the trap. The magnet's motion can also generate Eddy currents in the copper tracks of the trap. Both allow the magnet's motion to couple to the environment, further increasing the damping on its motion and reducing the potential quality factor. The total quality factor is a combination of the sum of the inverses of all quality factors:

$$\frac{1}{Q_{total}} = \sum_i \frac{1}{Q_i} \tag{2.10}$$

The quality factor (Q factor) is defined as the number of oscillations of a damped harmonic oscillator after which its amplitude has dissipated to $\frac{1}{e}$ of its starting amplitude. Equivalently the time constant τ of such an exponential decay is proportional to the Q factor. In our experiments we measure the driving and decaying of the motion of the magnet at one of

its resonances to see what is called a ringdown: its amplitude decreasing over time, i.e. the oscillator ringing down. By fitting an exponential decay to these measurements we find the time constant which together with the resonance frequency ($\omega_r = 2\pi f_r$) gives the Q factor:

$$Q = \frac{\omega_r \cdot \tau}{2} = \pi \cdot f_r \cdot \tau \tag{2.11}$$

2.3 Simulations

We have performed simulations of a double loop type Magnetic Paul Trap with *Python* of the motion of a point-like magnetized particle. Calculation of alternating trapping fields was accomplished using NASA's published analytical expressions for magnetic fields produced by closed loops [8]. The simulation is based on iterative calculation of the particles' position and rotation as well as force and torque exerted on it by the magnetic fields. We found the range wherein trap parameters, including current through the trap loops, inner loop to outer loop diameter, inner loop to outer loop current and trap frequency, lie to be very broad, narrowing the dimensions and parameters of a realistic trap down only vaguely. We found a homogeneous magnetic field necessary for stable levitation if the particle is allowed to rotate.

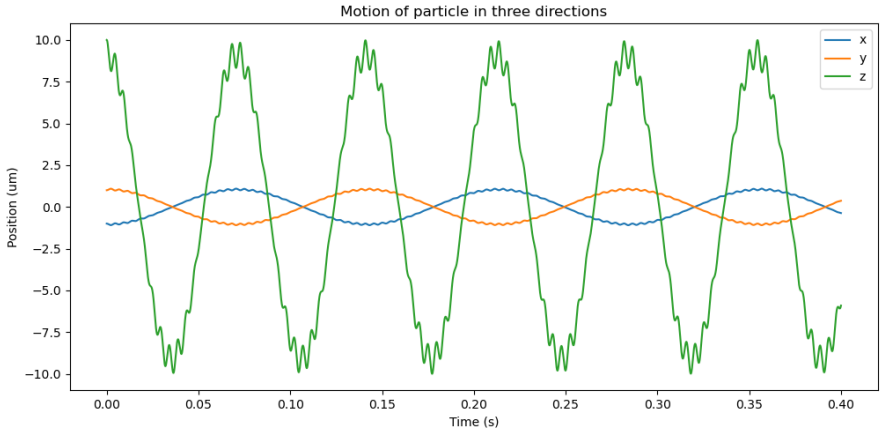

Figure 2.1: *Simulated motion of a point-like magnetized particle in three dimensions. As expected from Eq. 2.3 the center of mass frequency of the vertical motion is twice that of the planar motion. The particle moves with a secondary frequency, which is its response to the trap frequency. The initial offset is $z_0 = 10\mu m$ and $x_0 = y_0 = 1\mu m$ and the motion is not damped.*

3. EXPERIMENTAL METHODS

This chapter discusses the physical aspects of the setup we built in which we succeeded levitating our magnet of choice: a $Nd_2Fe_{14}B$, nickel coated cube magnet with sides of $250\mu m$. In a second section three techniques of measuring the motion of this levitated magnet are described, which were tested and of which the results can be found in Chapter 4.

3.1 The Magnetic Paul Trap

3.1.1 On-chip proposal

The proposal in [2] describes a trap based on magnetic fields in three parts: the outer and inner loops of an on-chip double loop structure carry an alternating current in opposite direction, with the outer loop diameter and current twice that of the inner loop, such that the fields (B_1) cancel each other in the middle of the trap. A magnetized particle will feel a potential well, which is most suitable for trapping when its alignment is along the axis of the loops. Alternating this field is necessary to push the particle back when it strays from its equilibrium, and the further it strays, the stronger the field pushes back. Aligning the particle's magnetization direction can be done by applying a homogeneous B_0. Additionally a field gradient $B_2^{'}$ can be applied to counteract for the gravitational pull on the particle to bring its equilibrium height to the center of the trap. We have borrowed the schematic figure used in the proposal 3.1 for clarification.

3.1.2 Our larger design and realisation

We applied the ideas of the on-chip proposal to a more manageable electronic structure printing technique: the printed circuit board. Apart from the double loop type trap we also put on an Anti-Helmholtz type configuration by printing on both sides of the board. We designed a 10cmx6cm PCB with four tracks: for both trap-types (double-loop, AHC) a $300\mu m$ track for traps with inner radius between $1mm$ and $2mm$ and a $200\mu m$ track for inner radii $1.1mm$ to $0.6mm$. See Fig. 3.2. At every loop location on the

board a hole is bored such that the magnet can move about freely around the center of the trap.

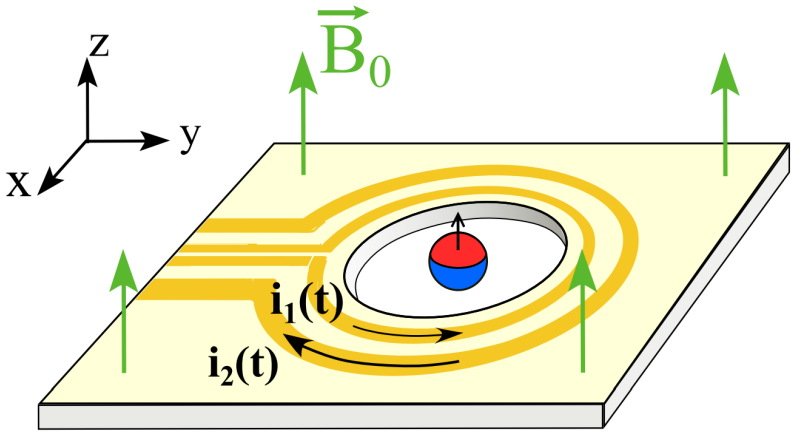

Figure 3.1: *Figure borrowed from [2]. The on-chip design for the Magnetic Paul Trap. A double-loop structure carries alternating current in opposite direction. A homogeneous magnetic field is generated along the axial direction of the loops. In our larger design the structure is realised on a printed circuit board and a cube magnet is used in stead of a spherical one. This schematic drawing represents the ratio between the magnet's diameter and the loop diameters of our realised trap ($\sim \frac{1}{6}$) well, despite this ratio being much smaller in the original proposal ($\frac{1}{100}$)*

The application of B_0 and B_2' was done by building a Helmholtz coil pair with radius and separation $14mm$ theoretically capable of creating several tens of milliTeslas (at 1 Ampere) in their common center, thus in the trap. Two *Tenma 72-2540* current sources individually applied current over both coils such that the aligning field and gradient field could be controlled. The trap is driven by an *Agilent 33220A* arbitrary waveform generator combined with a *Servowatt DCP 260/30A* AC current booster. The current is divided $\frac{1}{3}$ to $\frac{2}{3}$ over the inner and outer loops by two high power potentiometers, and the phase shift is accomplished by sending the current through the trap in opposite directions.

A specific aluminium plate (18cmx18cm) was manufactured for mounting all parts, with a hole in the middle that perfectly fits one of the Helmholtz coils. The board can be placed directly on top of the plate, such that the top Helmholtz coil is clamped tight on top of the board. A $1mm$ thick slab of teflon with a $1.5mm$ diameter hole centered over the trap is placed between the board and the top Helmholtz coil. Two thin cover glasses cover the inner cylindrical space on top and on the bottom confining the magnet

Figure 3.2: *A photograph of the front side of the Printed Circuit Board with our design for many differently sized double-loop configurations and (anti)Helmholtz configurations, which makes use of printing the second loop on the other side of the board. The loops with a larger diameter are printed with a track width of* $300\mu m$*, while the smaller traps are printed with a track width* $200\mu m$*. The track height is* $30\mu m$ *copper. Board material is standard FR-4. Our measurements were done in the 1.4mm wide double-loop trap.*

to this region prior to trapping. The aluminium plate is mounted on four 10cm high pillars placed on a base over which a glass dome fits forming a vacuum chamber.

3.2 Optical readout with camera

By mounting a camera (*Bresser MikroCam SP 5.0*) on a microscope we can observe and film a levitating magnet in our trap at a high enough framerate (between 300-500fps depending on brightness of surroundings) to see the magnet's motion, and subsequently see it's motion represented by peaks in the frequency domain. Our camera can be connected to a computer via USB, which makes storing data directly simple. To analyze the motion we used the OpenCV (Open Computer Vision Library, version 4.8.1) python packages to follow the motion of the magnet in a video. The library allows one to choose a tracker, open a video and draw a rectangle around the object that is wished to be tracked. Some tracker types are

better at following certain movement than others based on visibility and speed of the object's contours in the video, and choosing the wrong type often results in the tracker losing the object at some time during the video. For our video's the "CSRT" tracker (*Discriminative Correlation Filter with Channel and Spatial Reliability*) seemed to work best, as it never loses the object. See Fig. 3.3a.

An inherent downside to OpenCV's tracking possibilities is the fact that the boundary box can not rotate, does not fit tightly around an object and can only be a rectangle. To solve some of these issues we used the library's functions for finding objects in images, referred to as object detection. By grey scaling an image and defining the contour parameters for threshold- and maximum values all of the contours the function finds can be returned. By choosing the largest of these we found the contour around the magnet for every frame in a video successfully. This new boundary box shaping technique can rotate and fits around the image of the magnet tightly, resulting in better tracking and more accurate following of its center of mass. We also used functions present in the library to get the center of mass from any contour. See Fig. 3.3c.

Boundary box coordinates are saved after running the tracking through a video. From there it is straightforward to perform a Fourier transform and plot the data in the frequency domain.

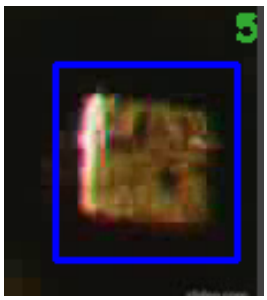

(a) *A still frame as taken from the built in OpenCV object tracking method. A Region of Interest is drawn by the user around the object that is wished to be tracked. The tracker then tries to draw a similar region around a similar object in consecutive frames.*

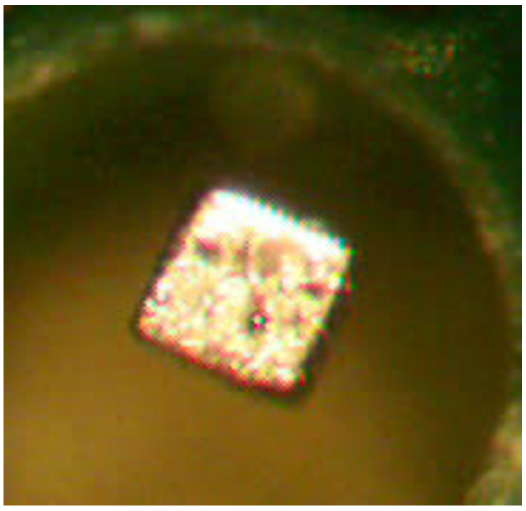

(b) *A still frame of the 250μm cube magnet being stably levitated in the Magnetic Paul Trap. The PCB trap structure is seen in the background.*

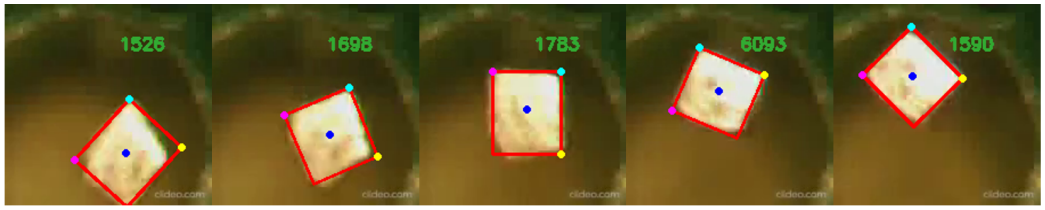

(c) *Five consecutive frames taken during motion tracking of the levitated cube magnet's motion. The object detection method is used here. We see that for every frame the tracker finds a rectangle shaped contour around the top of the cube, which is clearly visible in every frame. By tracking the location of the corners of this rectangle, we find its rotation around the z-axis, α. This rotation has a low frequency, however, and can be well approximated by eye. The blue dot is the center of mass of the rectangle, whose coordinates are used in analyzing the x- and y motion. The number printed in green is the number of frames the software can analyze per second and is, due to the low computing power necessary for this method, simply bottlenecked by the speed of the video.*

Figure 3.3: *The 250μm cube magnet as seen through a microscope and used in tracking analysis.* ***a.*** *OpenCV's built-in video tracking package.* ***b.*** *The levitating magnet hanging still in the trap, seen from above.* ***c.*** *Consecutive frames from our object detection tracker.*

3.3 Magnetic readout

A changing magnetic field induces a voltage in a coil. It should therefore be possible to pick up the vibrational motion of a levitating magnet with a so-called pick up coil. Ideal dimensions of a pick up coil are such that the greatest change in magnetic field is felt by the coil. A coil with size of the order of the magnet is suspected to do this. As our trap is magnetic, our pick-up coil will be prone to noise, but the smaller the coil, the smaller the picked up signal. Since our levitated magnet is $250\mu m$ wide it is difficult to construct a coil of a size similar to the magnet. For these reasons we construct a simple coil by winding $80\mu m$ insulated copper around the wooden end of a cotton swab spaced with plastic washers. The resulting coil has an inner diameter of $2mm$, an outer diameter of $5mm$ and a length of $3mm$. It has an induction of $100\mu H$ at $200kHz$. By placing the coil as close as possible to the trapped magnet and performing measurements with a *Stanford Research Systems SR830* lock in amplifier combined with an additional *Stanford SR560* low noise preamplifier, driving the particle (through the fields of one of the Helmholtz coils) at a range of frequencies and measuring the pick up coil's response, we should find a response around the magnet's resonances. See Fig. 3.4 for a picture of the setup. We calculate the expected induced electromotive force in a coil from the motion of the magnet as follows:

$$\varepsilon = -\frac{d\Phi_B}{dt} = -A_{coil}\frac{dB}{dt} = -A_{coil} \cdot \Delta B \cdot f_z \tag{3.1}$$

where ΔB the magnetic field change due to the motion of the magnet from one oscillation and f_z the frequency of oscillation. We calculate an induced voltage in the coil on the order of several nanoVolts.

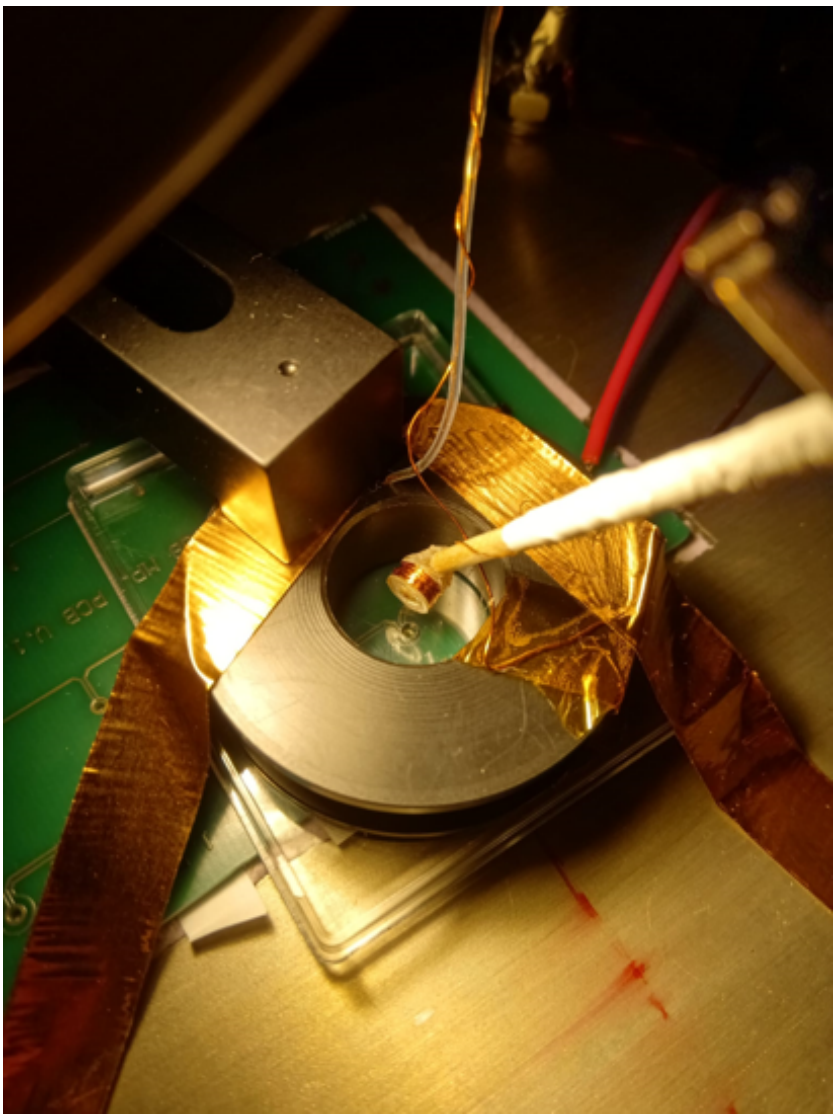

Figure 3.4: *A picture of our pick up coil being positioned near the trapped particle in the MPT setup. Just below the PU coil the structure on the PCB can be made out. A plastic spacer ($\sim 1mm$) and a glass cover are between the PCB and the top Helmholtz coil, of which the black plastic bobbin is seen being clamped tight to the table. Copper tape for thermalization of the Helmholtz coil connects the coil to the table.*

3.4 Optical readout with laser

An optical readout of the magnet's motion should have a better signal-to-noise ratio than a readout based on magnetic fields, since the trap itself is a collection of magnetic fields. A laser shining on the surface of the magnet creates a reflected beam or speckle pattern (depending on the surface roughness) that contains the motion of the magnet in its angle of reflection [9]. Alternatively the laser can be shone through the trap. The light at the photodiode then contains the magnet's shadow and therefore information about its motion. Fig. 3.5 contains a schematic drawing of the setup, in which the laser and photodiode emit and collect the beam horizontally, and the guiding of the beam through the trap is done with silver mirrors and positioning plates. We use a 4mW *Spectra-Physics model 102-3* He-Ne laser. A quadrant photodiode (a collection of four photodiodes in a 2x2 grid) can then be used to measure the total intensity of the arriving light as well as the lateral intensity in two directions. We used a *New Focus model 2901 visible quadrant cell photoreceiver* which has outputs for the total illumination (SUM), and two outputs for acquisition of the lateral position of a particle in the beam X and Y. From these signals a position can be found, but we only look at the frequency spectrum, therefore it is unnecessary to do this calculation. We have had two working setups; in the first all three channels can be read out through a *Rigol DS1104 Z+* oscilloscope connected to a computer while the particle driving is performed by a *Stanford SR830* lock in amplifier's output signal. In the second a *Zürich Instruments MFLI* digital lock in amplifier drove the particle and measured one channel of the photodiode at a time.

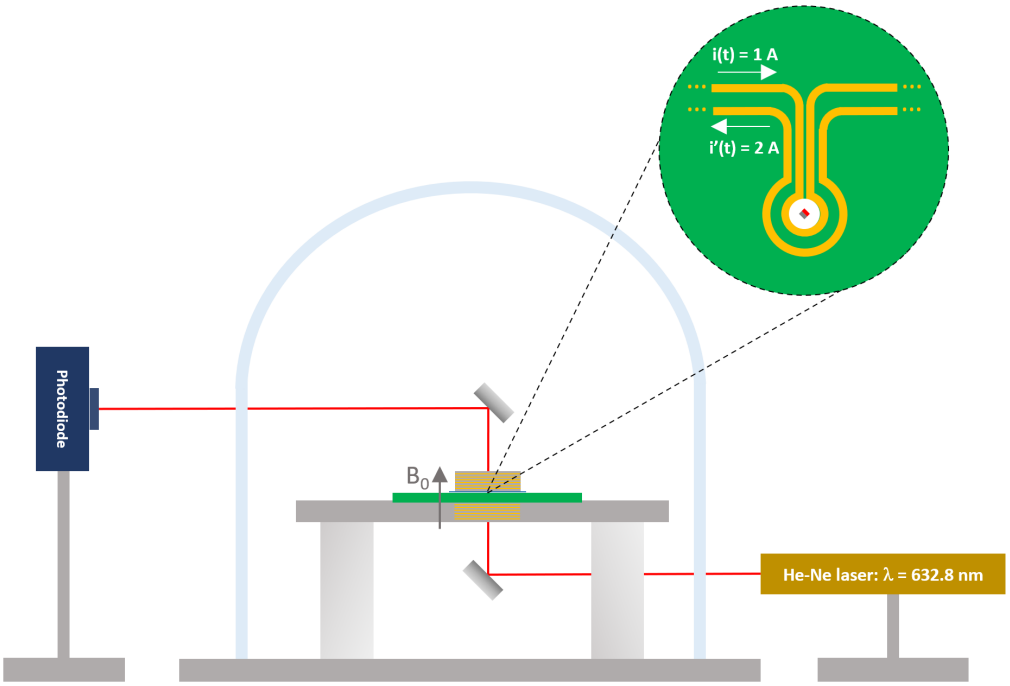

Figure 3.5: *A schematic representation of the setup with which we performed measurements by shining a laser through the trap onto a quadrant photodiode. The magnet's motion is picked up by the photodiode as a perturbation in the beam. The board with the trap structure is elevated to allow the placing of a mirror underneath it. In the plate on the posts is a slot in which the bottom Helmholtz coil fits. The top Helmholtz coil and a teflon spacer are clamped on the board. Two cover glasses cover the inside of the trap on the top and bottom, but allow the laser to shine through. This schematic represents nicely how a large vacuum chamber excludes certain types of read out techniques.*

4. RESULTS

4.1 Regarding trapping parameters and stability

Having an aligning field (B_0) and a field gradient ($B_2^{'}$) to counteract for the gravity on the particle proved indispensable for stable levitation. Without it the particle behaves chaotically in the trap, if it is confined in any way at all, else it flies out randomly. This chaotic behavior is key to our trapping, which is not an active loading technique where the magnet is placed into an equilibrium position deliberately, but rather is confined to an environment (cylindrical due to fabrication of the trap) in which the magnet flies around chaotically until it falls into the magnetic potential well by chance. Without generating B_0 and $B_2^{'}$, this never happens. Furthermore, with optimal trap settings, this happens more quickly, suggesting that optimal settings are those in which the potential well is deeper and overall more felt by the magnet. N.B. the magnet 'feels' the potential well best when its magnetization direction is aligned with the axial direction of the trap.

Levitation in our final measurement setup, which involved the laser and quadrant photodiode combination, required a much larger $B_2^{'}$ gradient to be stable, despite the trapping procedure being similar still. We attributed this to possible degradation of the Helmholtz coil pair from being loaded with hundreds of milliAmps while in vacuum. Their plastic bobbins, when melted, would alter the shape and/or position of the coils relative to the trap, which when not optimal can have significant effects. This presumption was confirmed after a measurement at low pressure ($P = 1.6e$–$2mbar$) where we kept the current through the Helmholtz coils much higher than in previous low pressure measurements to keep the trapping more stable, necessary to keep the magnet from falling out at low pressure. Afterwards we found the top Helmholtz coil's bobbin had melted and gotten deformed. The deformation was severe enough for the trap not to function anymore.

We have tried many of the sizes of traps on our PCB design, but only found stable levitation in the 1.5mm and 1.4mm traps, suggesting that the

	Value
B_0	8mT
$B_1^{''}$	30-40Tm^{-2}
$B_2^{'}$	0.5mTm^{-1}
$\omega_z = 2\omega_{x,y}$	$\sim (2\pi)20Hz$
$\omega_{\gamma,\beta}$	$\sim (2\pi)1000Hz$
ω_α	$\sim (2\pi)2Hz$
$r_1 = \frac{1}{2}r_2$	$0.7mm$
$I_1 = -\frac{1}{2}I_2$	$1.1A$

Table 4.1: *Estimates of the field strength, gradient and curvature of the three generated fields in the Magnetic Paul Trap as well as the working trap frequency range and the resulting mode frequencies, although the librational $\omega_{\gamma,\beta}$ is calculated and has not been observed yet. B_0 was measured with a Gaussmeter. $B_1^{''}$ is calculated using Eq. 2.3 and the fitting parameters from Fig. 4.4. $B_2^{'}$ is calculated based on B_0 of both Helmholtz coils and their distance of separation.*

ideal ratio for a cube magnet in loop-based MPT lies around 1/6 magnet width to inner trap diameter. In a smaller trap the magnetic potential well becomes too narrow for a large magnet to fit in, while a larger trap requires lots more current to produce an equally deep well as a smaller trap, since the strength of the trapping field reduces by the third power with distance. We observed burning of the PCB tracks from 3.5 Amperes, therefore we limited ourselves to the working $I_1 = -\frac{1}{2}I_2 = 1.1A$ to prevent acute heat damage and damage over time. The current through both trapping loops was constantly measured as it had been set up to divide the current over the inner and outer loop.

4.2 Measuring techniques

4.2.1 Optically with camera

Different read out techniques were set up to measure the levitating magnet's movement and subsequently its eigenfrequencies. Viewing the magnet with a camera through a microscope proved to be a technique able to measure all spatial modes of the trapped magnet, thanks to proper visibility and high-enough framerate. It lacked however in its ability to measure the librational modes, as it is estimated that these modes reside at frequencies around $1000Hz$, and a very high framerate would be needed to see these modes. Furthermore, application of camera-through-microscope observation of the trap is practically infeasible in our setup when the setup is converted to the depressurization chamber that was available to us. Also, data obtained with this method is in the form of video-capture and analyzing these through the use of video tracking is cumbersome, albeit doable.

In our analysis, we have used two methods of finding a frequency spectrum of the motion of our trapped magnet, both making use of the open source video-analysis Python library *OpenCV*. The first method relied on the existing trackers accessed through this library, while the other made use of the object detection features of the library, usually done on images, but for this application was implemented on video. Fig. 3.3a holds a still of the first method, in which a rectangle shaped Region of Interest is drawn by the user, which is then redrawn in subsequent frames by the tracker. The pixel coordinates of the rectangle are saved and used for analysis. The inherent two-dimensionality of video-capture results in the axes of recordings not being aligned with the axes of the modes of the magnet. Therefore, the x- and y coordinates of the boundary box drawn by the tracker hold projections of the magnet's movement on the video axes, but by rotating the data in post we can align these axes. Under an angle (3.3a) all three spatial modes are projected on to the video's two axes.

Fig. 4.1 shows the frequency domain of the motion of the magnet as filmed directly from above on the left, and filmed under an angle on the right. Two frequency representations are presented, one of the motion along the horizontal axis of the video and the other along the vertical. We see in total three modes appearing in the data. During the filming of both videos used in this analysis the magnet's motion is excited through minor perturbations (lightly tapping the setup). Two resonances are found in the topview image, one stronger than the other, at $8.5Hz$ and $14.2Hz$. Under an angle we also see a $24.4Hz$ resonance. During these measurements we have observed individual spatial mode excitation by driving the magnet

at these frequencies.

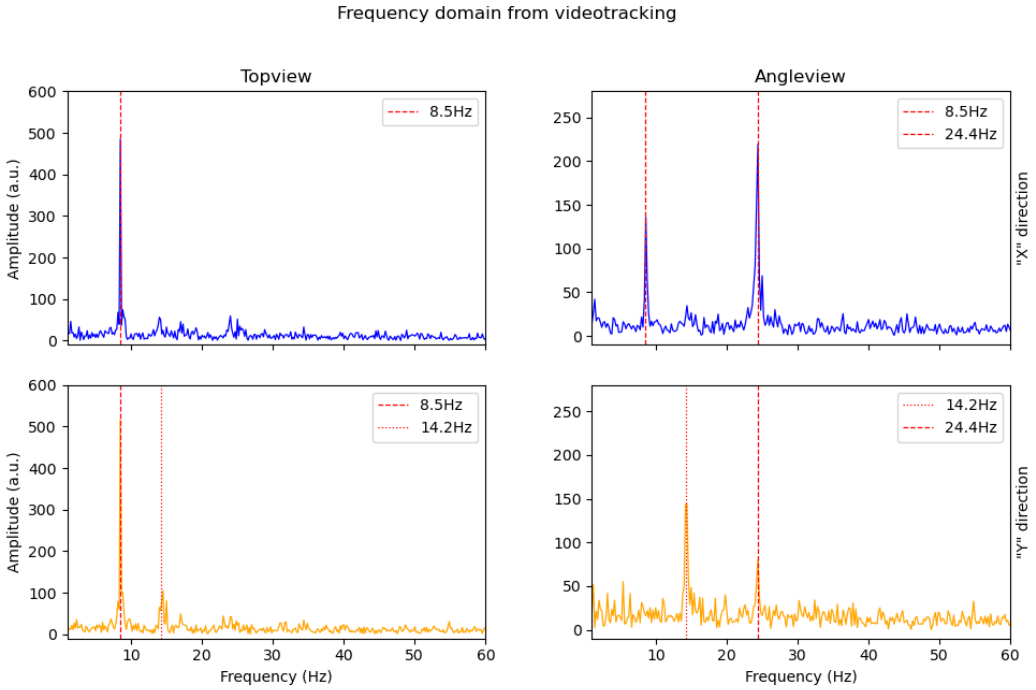

Figure 4.1: *The frequency domain of the equilibrium motion of the magnet at room temperature and ambient pressure, measured by object tracking and split into double columns and rows specifying the camera angle and the video coordinate axis along which the Fourier transform was taken. Assuming the two axes (vertical, horizontal) of the analyzed video do not share the orientation of the x- and y modes' directions in the actual trap, the data is rotated to make these axes align. We see however that the motion is a collection of modes such that they never appear on individual axes only. The z-mode is visible in the recording under an angle, as expected, while it is absent when the magnet is viewed directly from above. Trap settings:* $\Omega = 223Hz$, $I_1 = 4.8V$.

4.2.2 Pick up coil

The pick-up coil as described in Methods was unable to give a good signal to noise ratio for more than one mode at a time. This is due to the spacing of the coil relative to the trapped magnet, which determines the coupling to modes. At most one mode with good coupling was achieved, with other modes being only barely visible. Much crosstalk between the pick up coil and the $B_{0,2}$ generating Helmholtz-coil pair lowered the SNR of this method. With the pick up coil placed semi-horizontally and as close as possible to the trap we obtain the results in Fig. 4.2. Since we have $V = IR$, Eq. 2.7 and Eq. 2.3 give a linear relation expectation for the voltage over the trapping loops and the spatial eigenfrequencies of the magnet. In Fig. 4.2 we have drawn a linear relation over the clearest continuously visible peaks, for which $V \sim 0.33f$. Two other traces of linear behavior might be present in the range 15Hz to 20Hz and 30Hz to 40Hz, of which the second could be a consequence of aliasing of the first response's signal.

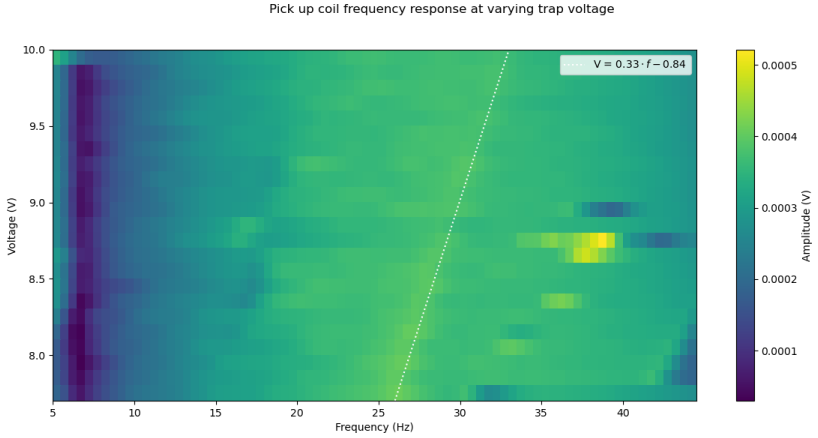

Figure 4.2: *The magnet's response to being driven at frequencies between 5Hz and 45Hz at varying trap amplitudes ranging between 7.7V ($I_1 = 0.85A$ and 10V ($I_1 = 1.10A$). A linear relation between the trapping current and the frequency of the eigenmodes is best visible from the shifting peak amplitude between 26Hz and 32Hz.*

4.2.3 Optically with laser

The laser and quadrant photodiode combination proved a good read-out technique of the magnet's motion. The implausibility of crossover between the photodiode's output and a lockin amplifier's output signal driving the magnet made it possible to measure the magnet's motion's frequency spectrum and its dependence on the trapping parameters with good signal to noise ratio. Artifacts are continuously present in all datasets, but varying the parameters in our setup for which the theory predicts an eigenfrequency dependence allows differentiating between signal and noise. Figs. 4.3, 4.4 and 4.5 show the response of the mode frequencies on a change in top Helmholtz coil current, trapping frequency and trapping amplitude (trap-loop current) respectively. The figures represent the response signal during subsequent frequency sweeps, each with the respective parameter slightly lower. In Figs. 4.5 and 4.4 two peaks in the frequency domain are at a different frequency for every parameter change.

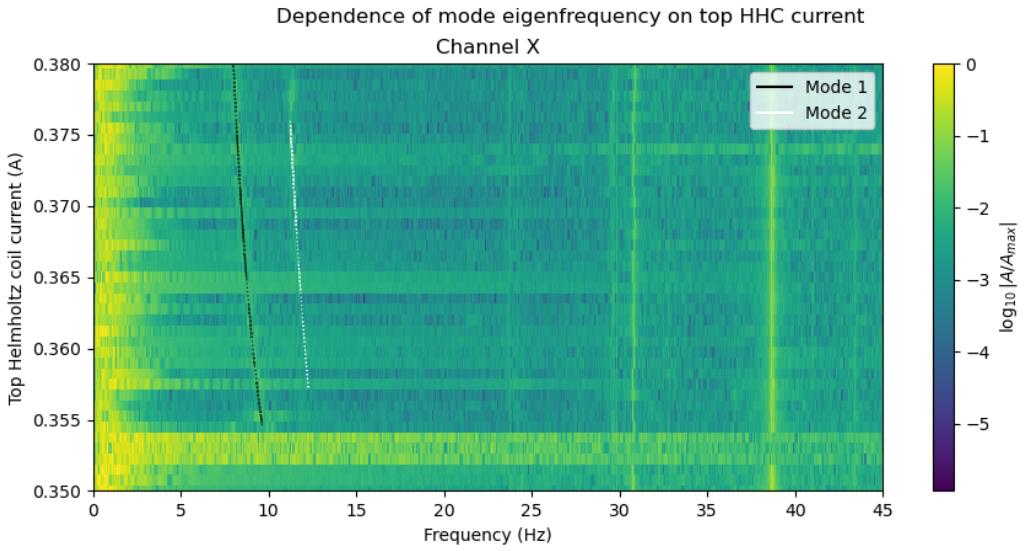

Figure 4.3: *A colormap of the magnet's response at frequencies between 5Hz and 45Hz at varying top Helmholtz coil current, which changes the levitation height of the magnet through varying the gradient (Eq. 2.9). Aside from artifacts which are consistent throughout the sweep, we see again see two modes like in Fig. 4.4 and Fig. 4.5. We've found an inverse 5^{th} power relation (which is plotted) between the current and the resonances to fit better than a first or a second, implying that the levitation height is in the range $z > R$ (Eq. 2.6, Eq. 2.7a).*

We fitted the expected relationships between the magnet's CoM frequency $\omega_{x,y,z}$ and the trap frequency Ω as well as the trap current (through

the curvature $B_1^{''}$). This was done by means of a double sliding window: a window is defined that follows the region around the peak linearly. The total curve to which we want to fit lies in the window, but other signals do not. For every frequency sweep a Gaussian is fit to the data in that window, such that we find the location of the peak for that sweep. Continuing this through the changing parameter we fit the expected relation to the collection of peaks found within the windows. This is done for both of the curves which we expect to be modes.

The results of a measurement in which we changed the $B_2^{'}$ gradient by control over the current through the top Helmholtz coil are presented in Fig. 4.3. We assume a linear relation between this current, the gradient field $B_2^{'}$ and the equilibrium height of the levitated magnet. We expect an inverse power relation between the equilibrium height and the curvature $B_1^{''}$ and thus the CoM eigenfrequencies $\omega_{x,y,z}$ (Eq. 2.3, Eq. 2.7). We've performed the fitting procedure as discussed before to fit $I \sim \frac{1}{f^x}$ for $x \in 1, 2, 5$ and found $x = 5$ the best fit, as evaluated by comparison of the shapes of the fit and data. This corresponds to Eq. 2.7a; the region of equilibrium height above the trap for which $z > R$.

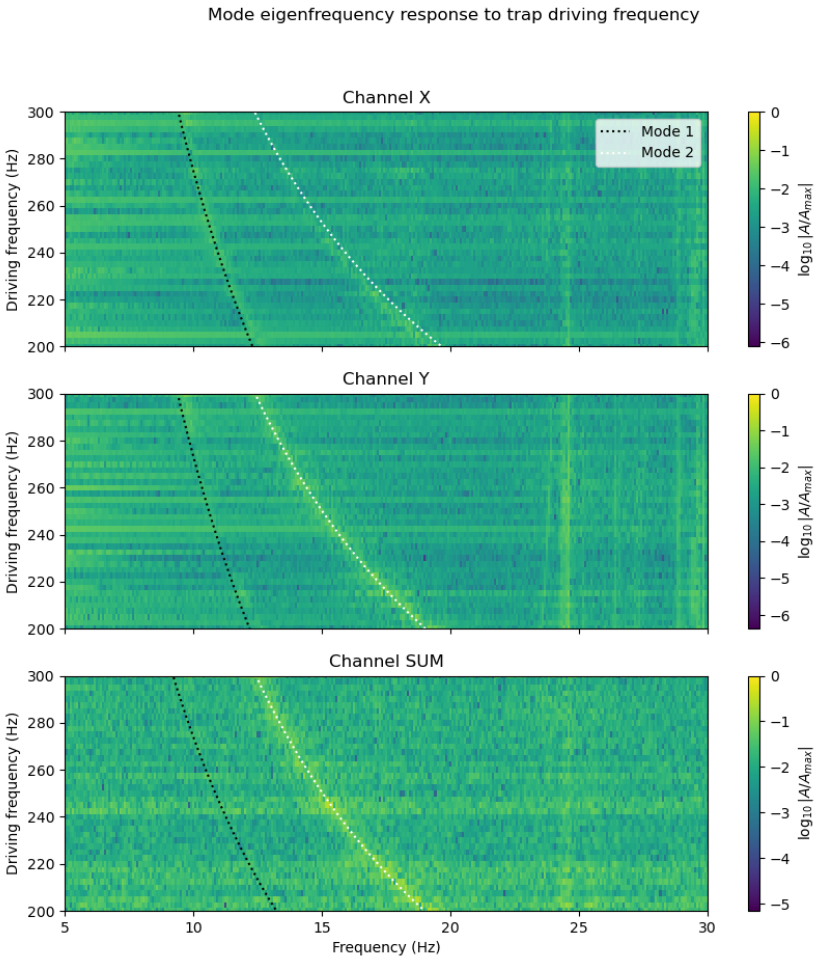

Figure 4.4: *A colormap of the three photodiode outputs X, Y and SUM in which the response of the magnet to being driven at frequencies between 5Hz and 30HZ is plotted for trap driving frequencies between 200Hz and 300Hz. The expected relation between a mode frequency and the trap frequency is inversely proportional (Eq. 2.3). The fits show that the data represents such a relation. Individual channels represent the modes' visibility differently: Mode 1 is stronger in channel X, mode 2 is stronger in channel Y and SUM. Consequently the fits on mode 2 in channel X and mode 1 in channel Y are a bit off. These sweeps were done at a trapping amplitude of 5V ($I_1 = 1.1A$).*

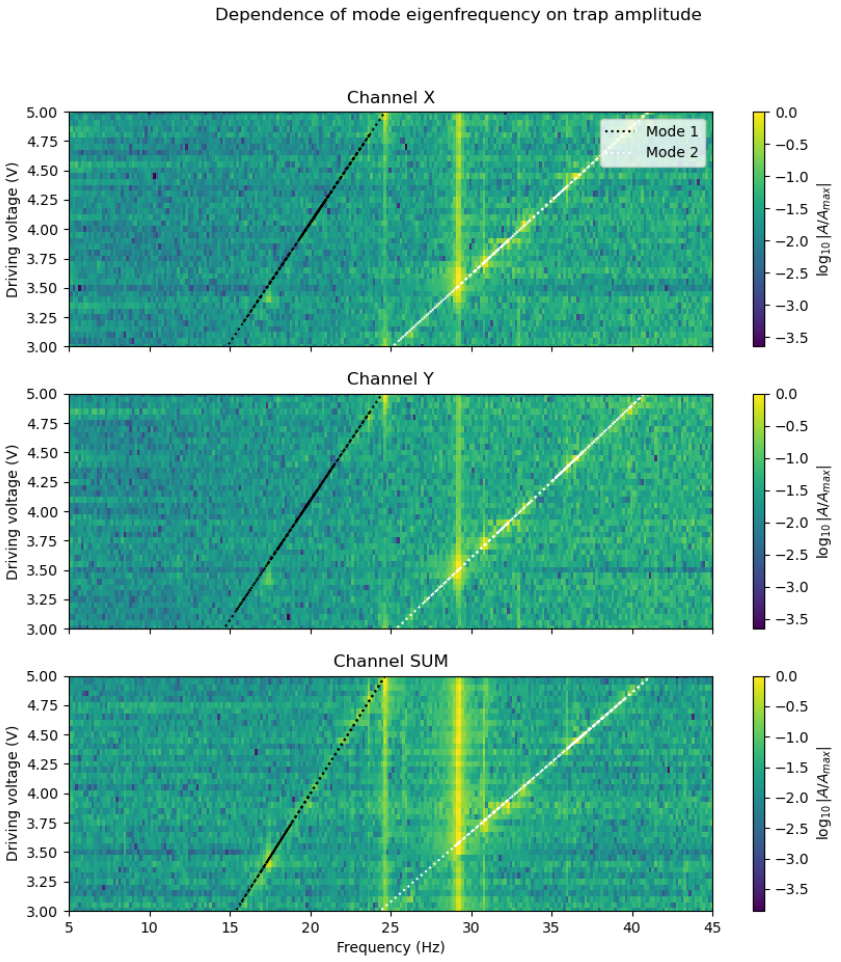

Figure 4.5: *A colormap of the three photodiode outputs X, Y and SUM in which the response of the magnet to being driven at frequencies between 5Hz and 45HZ is plotted for trap driving amplitudes between 3V and 5V. This relation is expected to be linear (Eq. 2.3 and Eq. 2.6), which is what we see after fitting a linear relation to the data. Artifacts around 25Hz and 29Hz are strong, but are consistent throughout changing the trap parameters, therefore it is unlikely that they are due to the trapped magnet. These sweeps were done at a trapping frequency of 287Hz.*

4.2.4 Damping

A collection of ringdown measurements at varying pressure is seen in Fig. 4.6. We see two ringdowns at ambient pressure, which are the result averaging 10 ringdowns in succession and fitting exponentially, acquired once through channel Y and once through channel SUM of the quadrant photodiode. Similar values for the time constant of each ringdown are found from the exponential fit on the data. The levitating magnet was not driven to the same amplitude, as is seen from the differing amplitude of the oscillation at $t = 0$. This is because we increased the driving amplitude only after observing that the magnet was still trapped and had not been kicked out of levitation by the driving.

Our vacuum pump, a *Pfeiffer Vacuum HiCube*, depressurized the system to a stable pressure of $1.6e0mbar$ without the turbopump and to a stable $P = 1.9e\text{–}2mbar$ with the turbopump active. Only a single succession of ringdowns was performed at the lowest pressure, as we tried to prevent too much heating from destroying the trap. A low driving amplitude was used to make sure the magnet would stay trapped.

In Fig. 4.7 a ringdown as measured optically by camera is presented. The magnet was driven by tapping the setup. Therefore all CoM modes are excited and the motion is collective. The view in the analyzed video of this ringdown is from the top. As a result the z-mode is not observed. The motion is a collection of modes, which is concluded from the fact that there is no rotated planar coordinate system for which the x- and y modes can be individually projected on the video axes. From a manual fit to the amplitudes of the oscillations we find a time constant of $1.5 \pm 0.2s$, which gives a quality factor (Eq. 2.11) $Q = 52.4 \pm 3.5$.

We have collected the resulting quality factors and the pressures at which they were found in Fig. 4.8. The point found in Fig. 4.7 is presented in blue. The remaining six from Fig. 4.6 are red.

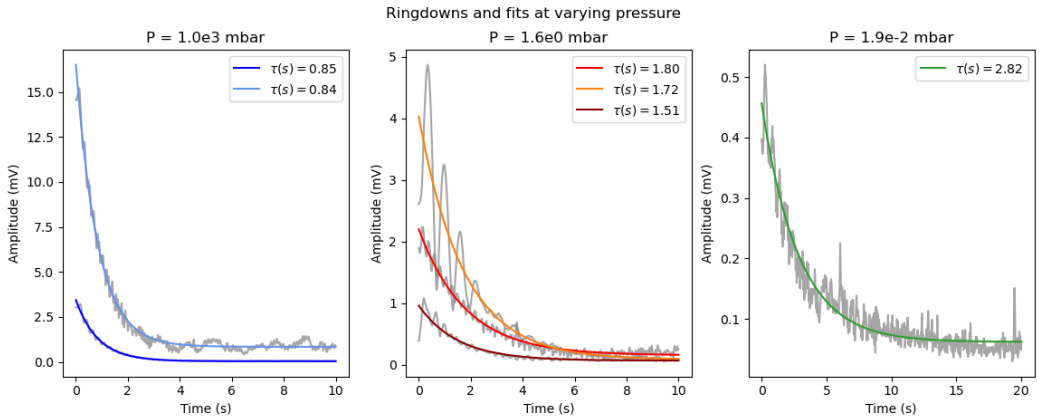

Figure 4.6: *Ringdowns measured with the laser and photodiode setup, performed by driving the magnet at a resonance frequency and allowing it to ring down while measuring the response over time. Each data in grey is an average over 10 ringdowns taken within the same measurement with the same settings, and the various ringdowns within the subfigures signify distinct measurements with different driving amplitudes (which results in different ringdown amplitude) and resonance frequencies (due to inconsistencies of the trap, as well as having to re-trap the magnet and the resulting difference in settings). Exponential fits over these averages are presented which show that the time constant increases with decreasing pressure, signifying that the gas damping on the magnet reduces. The fit-certainty gives a time constant error of* ± 0.02 *at the most.*

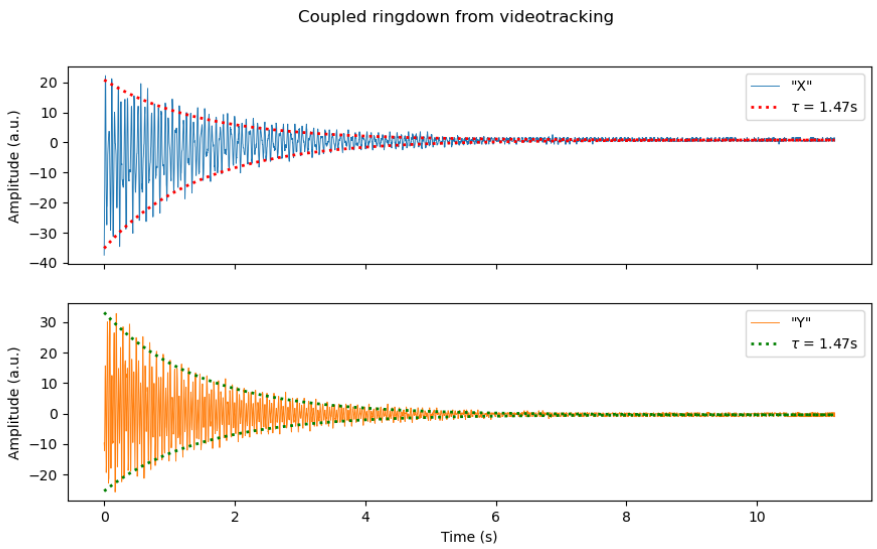

Figure 4.7: *The motion of the trapped magnet as projected onto the horizontal and vertical axes of a video recording, during which the setup was lightly tapped to excite the magnet slightly, such that a ringdown can be seen. Vibrations of the setup ring down much quicker than those of the magnet, and the data visible here is that of a second after tapping, such that only the magnet's motion should be taken. A manual exponential fit to the amplitude of the oscillation results in a time constant of* $\tau = 1.5 \pm 0.2s$*, which gives* $Q = 52.4 \pm 3.5$*. Due to the nature of the excitation all modes are excited. The video was taken from directly above such that the x- and y mode are most visible. The x- and y modes have different Q factors, as they have different resonance frequencies. The resulting Q is collective for these modes.*

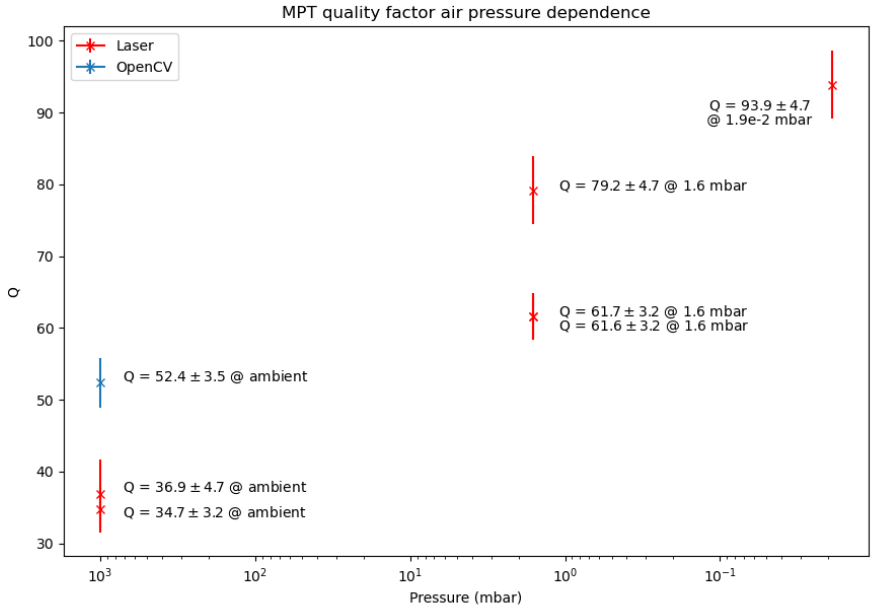

Figure 4.8: *A collection of datapoints relating the quality factor of our levitating magnet to the air pressure of its environment. The points in red are obtained with the laser+photodiode method, while the single blue point is from Fig. 4.7. Although an inversely proportional relation between the quality factor and the pressure is expected this is not immediately reflected by the points. Despite the lack of additional data clarifying the result, it is not unthinkable that gas-damping is only a small part of the total damping, since our Q is very low already, and much higher Q's for magnetically levitated particles have been reported [10–13].*

5. Discussion

5.1 Trap dimensions and settings

Our results show that our Magnetic Paul Trap with double loop design can stably levitate a $250\mu m$ NdFeB magnet for several hours. Despite our initial idea of the necessary large current through the trap structure required for levitation, only $\sim 3A$ through both loops is needed for levitation in our setup and this can be lowered after trapping the magnet. This provides hope for further miniaturization of this trap design. Decreasing the size of the trap to chip size will reduce the maximal current one is able to send through. Placing the trap in a cryogenic environment might be wanted in the future, which further increases the difficulty of sending high currents through the system. As these limitations might not scale with the reduction of the necessary current as the design is miniaturized, the result of not having to send a too large current in our setup is welcome.

The size ratio between the trapping loops and the particle we succeeded to levitate lies around $w = \frac{d_1}{6}$ with d_1 the diameter of the inner loop and w the width of our magnet. In the first design for levitating a radius $1\mu m$ spherical magnetized particle an inner loop radius for the trap structure $r_1 = 100\mu m$ is proposed. We have suggested that at larger ratio of trap-loop radii to particle size the necessary current for levitation skyrockets, but this would have to be checked. This experiment can readily be performed in our setup by attempting levitation in the larger traps on our PCB. Current around $|I_1| + |I_2| \sim 4.5A$ will burn out the tracks on the board, but more thermally conducting materials are available (Aluminum Oxide as a board material, for example).

5.2 On the motion in levitation

Observing the magnet through a microscope shows most reliably that the frequency responses are the magnet's spatial modes; we have driven the magnet at its resonances and observed individual mode excitation. Trapping-parameter dependent measurements show that we can shift the magnet's

resonances. The fits to Fig. 4.4 and 4.5 are good and show that the eigenfrequencies of our system behave according to Eq. 2.3. From the fitting parameters and Eq. 2.3 we extract a value for $B_1^{''}$ in our system and find it is four orders of magnitude lower than predicted in a similar on-chip design of the trap [2]. This is realistic, as our trap is larger in size and curvature of the trap-generated field should be weaker.

In Fig. 4.6 we attribute the frequency shift that we observe between the measured ringdowns to trap instability and having to re-trap at slightly different settings in between measurements. It is also possible that we are seeing a frequency pulling effect [11, 14]. The resonance frequencies shift with the amplitude of the oscillation. Each time we perform a ringdown by driving at a different amplitude we change the starting eigenfrequencies of the mode we measure, which during the ringdown shifts back. This phenomenon should in future experiments be researched further if we wish to understand our system better.

Comparing trap amplitude dependent measurement with the pick up loop in Fig. 4.2 and with the laser in Fig. 4.5 we find a similar slope: the first has $V \sim 0.33f$, while the second has $V \sim 0.17f$. Noting that in the earlier experiment we used a peak voltage instead of a peak-to-peak voltage, therefore the voltage in the first figure is double the voltage in the second figure, but corresponds to the same current through the trap. We conclude that the slopes Mode 2 in Fig. 4.5 and the fit in Fig. 4.2 are the same mode. Therefore, the signal in Fig. 4.2 (in the range 15Hz-20Hz) that looks like a linear response can be associated with Mode 1 in Fig. 4.5. It is worth noting this similarity between the results of two different types of measurements (magnetically and optically). The mode frequencies we measure optically in other parameter dependent experiments as well as in the results from the video tracking analysis are similar amongst themselves but lie about 10Hz lower. It is not clear what causes this discrepancy. It is unlikely that the highest lying mode in Fig. 4.5 and Fig. 4.2 is the z-mode, as it should then also be visible in other laser acquired results. Instead in those figures (Fig. 4.4 and Fig. 4.3) we see the same x- and y modes as we observed with the camera (Fig. 4.1). Through replication of these findings in further measurements we might come to a better understanding of this discrepancy.

For the gradient dependence we expected to find the levitation height from a relation between the top Helmholtz coil current and the shifting of the eigenmode frequencies. The far-from-the-loop regime corresponds best to the data. However, this implies that the equilibrium height of the magnet is further than $r_1 = 0.7mm$ from the trap, which is not possible as

the height between the cover glass and the board is $1mm$. With a microscope we have observed the magnet's equilibrium height to be close to the trap structure on the board. We can further investigate this problem by considering the offset due to the gradient using Eq. 2.9. A similar approximation can be made for the negative offset due to gravity. We know our Helmholtz coils generate a typical gradient of around $B_2^{'} \approx 0.5mT/m$:

$$z = h_g + h_{mag} \tag{5.1}$$

$$h_g = -\frac{g}{\omega_z^2} \tag{5.2}$$

$$h_{mag} = \frac{F_{mag}}{m\omega_z^2} = \frac{\mu B_2^{'}}{m\omega_z^2} = \frac{B_{sat}B_2^{'}}{\rho_m \mu_0 \omega_z^2} \tag{5.3}$$

where we have used the norm of the magnetic moment of the magnet $\mu = \frac{B_{sat}V}{\mu_0}$ and in which g the gravitational acceleration. We find $|h_g| \approx 600\mu m$ and $|h_{mag}| \approx 4\mu m$. Certainly the gradient we measured can not account for the offset that predicts the far-away regime (Eq. 2.7a) which we see in the data. At the same time the predicted gravitational offset is much larger than what is realistic. If the magnet would levitate more than several times its own size below or above the trap, we would have been able to see this in our microscope setup. We conclude that our model is too simplistic to describe the complex behavior of our system. The eigenfrequencies of our levitating magnet scale with a higher order to the levitation height despite the magnet not being in the regime where the curvature of the loops scale with this order. Our model does not account for the shape of the magnet and its protrusions off of the z-axis into regions where the fields are no longer described by our model.

The strength of the homogeneous B_0 produced by the Helmholtz coil pair was measured with a Gaussmeter and is similar to the field in the proposal [2]. The librational modes $\omega_{\gamma,\beta}$ are dependent on the strength of the aligning field. We have invested little time finding the librational frequencies with the laser and photodiode setup and found direct results lacking. To improve the visibility of the librational modes in the signal, the setup can be altered such that the reflection of the laser on a side of the magnet is picked up by the photodiode. Finding the librational modes would speed up measurements significantly, as these were limited by the low spatial eigenfrequencies of our system. From Eq. 2.4 we know $\omega_{\gamma,\beta} \approx 1000Hz$.

5.3 On the damping

Fig. 4.8 sums up our measurements regarding the lowering of the total damping by depressurization of the system. If the levitated magnet was mostly limited by gas damping, we should see an inversely proportional relation between the quality factor and the pressure. This is not what we see. Due to our lack of datapoints however, it is difficult to conclude any proportionality. We can conclude that other damping factors play a significant role in our system and are to be addressed if we wish to further increase the quality factor.

In [2] (Supplementary Materials III) it is shown that the current induced by the trapping loops onto each other is negligible. They also show that dissipation of Eddy currents generated in the magnet do not cause problematic heating even at high vacuum. Following the same approximation for this dissipated heat for our larger magnet we find

$$P = \Omega^2 \sigma a^9 B_1''^2 \sim 10^{-24} W \tag{5.4}$$

where σ is the electrical conductivity of NdFeB, the (bulk, the coating is more conductive) material. We draw the same conclusion for our larger particle.

A possible contributor to the damping is the induction of the moving magnet on to the trap loops, as well as generation of local Eddy currents. These effects couple the magnet to its environment. The energy stored in one oscillation of the magnet equals

$$E_{osc} = \frac{1}{2} m \omega_{CoM}^2 \delta^2 \sim 10^{-13} J \tag{5.5}$$

where δ the oscillator length which is on the order $10\mu m$ for small perturbations and relatively still motion. We calculate the power dissipation from the induced voltage in the loop (Eq. 3.1, $V \sim 1nV$):

$$P = \frac{V^2}{R} \sim 10^{-16} W \tag{5.6}$$

which gives an energy loss per oscillation of $10^{-4} E_{osc}$ at $10Hz$, which is insignificant.

We calculate the Eddy current dissipation from the Lorentz force acting on the magnet due to the motion of its perpendicular fieldlines in the copper tracks which contain free electrons:

$$F_{lorentz} = q(\boldsymbol{v} \times \boldsymbol{B}) = q \cdot v_\perp \cdot B_z \tag{5.7}$$

where $q = Ne$, the number of free electrons times the charge per electron. We calculate the effect of the planar movement of the magnet denoted by its speed $v_\perp$. We obtain the strength of B_z at the inner loop by the analytical description for the magnetic field of a cylindrical permanent magnet [15]. We find an expression for the dissipated energy in one oscillation of planar motion by Eddy current damping:

$$E_{Eddy} = qB_z \int v_x dx \sim qfB_z\delta^2 \sim 10^{-12}J \tag{5.8}$$

Where $B_z = 1mT$, $q = 0.54C$, $\delta = 10\mu m$, $f_\perp = \frac{\omega_\perp}{2\pi} \approx 10Hz$. The calculated possible dissipation through Eddy current damping is large enough to explain the damping we see at low pressure. To counteract this effect the distance between the levitating particle and the trapping loops would have to be increased. Problematically this requires increasingly larger currents to create the same field in the middle of the trap. The Eddy damping is proportional to the oscillator length squared. Miniaturization of the Magnetic Paul Trap is therefore expected to further decrease problematic Eddy current damping. Another possible solution of reducing Eddy damping in the Magnetic Paul Trap is using NdFeB magnets with a non-conductive coating, which are available to us.

From Fig. 4.8 we can deduce approximations for the quality factors in the mostly gas damped regime and in the mostly Eddy current damped regime. Using Eq. 2.10:

$$\frac{1}{Q_{total}} = \frac{1}{Q_{gas}} + \frac{1}{Q_{Eddy}} \tag{5.9}$$

we read from Fig. 4.8 $Q_{total} \approx 40$ at ambient pressure and $Q_{Eddy} \approx 90$ at low pressure. We deduce $Q_{gas} \approx 70$ at ambient pressure. We conclude that the Magnetic Paul Trap suffers almost equally from Eddy current damping as it does from gas damping at ambient pressure. Our calculations support this. Measures to reduce the Eddy damping effect will have to be taken if the quality factor is to be further increased. For a similar sized permanent magnet levitating above a lead superconductor [12, 13, 16] in a cryogenic environment similar eigenfrequencies are found, but Q factors are reported around $Q \sim 10^6$. In [16] Eddy current damping limited the quality factor of the system to $Q \sim 10^4$. The Magnetic Paul Trap suffers from stronger limitations due to the nature of the environment of a trapped particle in such a trap.

5.4 Noise

Persistent noise in our measurements is seen at 24Hz, 28Hz, 31Hz and 39Hz. This noise could interfere with read out of motion whose modes lie close or at the same frequency. To prevent this in future experiments the sources of the noise are to be addressed. In our final setup, in which we read out the motion of the trapped magnet optically with the laser and photodiode, the pillar-mounted table on which the trap resided was placed loosely on the base of the vacuum chamber. The vacuum chamber base is placed on a damped optical table, but is not secured to it. The laser and photodiode are both tightened to the optical table. To reduce noise in future measurements we suggest a workaround to securing the setup whilst keeping the vacuum chamber between the table and the trap. Boring half-way threads in the base of the vacuum chamber would allow securing the setup to it. The base has connections for its rubber feet at the corners, which could be connected to the table instead.

6. Conclusion

We have shown that our double loop type Magnetic Paul Trap design can levitate a sub-millimeter sized NdFeB permanent magnet at room temperature for long periods of time ($>$ 1hour). This trap allows the study of magnetically levitated particles at a practical scale without the need for cryogenic environments. The Magnetic Paul Trap has better control over a levitated particle than in comparable Meissner levitated systems [12, 13, 16], as we can control the resonance frequencies as well as the levitation height, similar to [11]. However, this high control is met with considerably larger damping due to Eddy current generation by the magnet's motion in its environment. Possible methods of reducing these have been discussed in the previous chapter. Before further measurements can be performed the B_0 and $B_2^{'}$ generating Helmholtz coils will have to be replaced. Then, laser optical read out measurements can verify the reproduction of the trapping we observed before the degradation of the Helmholtz coils. It might prove fruitful to rethink the setup: read out of a speckle pattern in the laser beam's reflection on the surface of the particle could increase visibility of the librational modes, allowing speedier measurement. Other side-questions remain; can we increase the distance between magnet and trap loops, to decrease Eddy damping, by adding more loops to the trap? Can we trap smaller magnetized particles in the smaller traps that are already on the printed board? Can we combine control over our particle with better environmental isolation by making the trap superconducting, e.g. on-chip? We leave these questions to future research.

BIBLIOGRAPHY

[1] C. Gonzalez-Ballestero, M. Aspelmeyer, L. Novotny, R. Quidant, and O. Romero-Isart, *Levitodynamics: Levitation and control of microscopic objects in vacuum*, Science **374**, eabg3027 (2021).

[2] M. Perdriat, C. Pellet-Mary, T. Copie, and G. Hétet, *Planar Magnetic Paul Traps for Ferromagnetic Particles*, (2022).

[3] J. Oppenheim, *Is it time to rethink quantum gravity?*, (2023).

[4] S. Bose, A. Mazumdar, G. W. Morley, H. Ulbricht, M. Toros, M. Paternostro, A. A. Geraci, P. F. Barker, M. Kim, and G. Milburn, *Spin Entanglement Witness for Quantum Gravity*, Physical Review Letters **119** (2017).

[5] F. Hanif, D. Das, J. Halliwell, D. Home, A. Mazumdar, H. Ulbricht, and S. Bose, *Testing whether gravity acts as a quantum entity when measured*, (2023).

[6] J. Gieseler and J. Millen, *Levitated Nanoparticles for Microscopic Thermodynamics - A Review*, Entropy **20** (2018).

[7] Q. Li, J. Goosen, F. van Keulen, and J. van Beek, *Gas ambient dependence of quality factor in MEMS resonators*, in *Proceedings of the IEEE Sensors 2009 Conference, 25-28 October 2009, Christchurch, New Zealand*, edited by Makhopadhyay, S.C., pages 1040–1043, IEEE Society, 2009, IEEE Sensors 2009 Conference ; Conference date: 25-10-2009 Through 28-10-2009.

[8] J. C. Simpson, J. E. Lane, C. D. Immer, and R. C. Youngquist, *Simple Analytic Expressions for the Magnetic Field of a Circular Current Loop*, Technical report, NASA, 2001.

[9] T. Delord, P. Huillery, L. Nicolas, and G. Hétet, *Spin-cooling of the motion of a trapped diamond*, Nature **580**, 56â59 (2020).

[10] M. G. Latorre, J. Hofer, M. Rudolph, and W. Wieczorek, *Chip-based superconducting traps for levitation of micrometer-sized particles in the Meissner state*, Superconductor Science and Technology **33**, 105002 (2020).

[11] M. Gutierrez Latorre, G. Higgins, A. Paradkar, T. Bauch, and W. Wieczorek, *Superconducting Microsphere Magnetically Levitated in an Anharmonic Potential with Integrated Magnetic Readout*, Phys. Rev. Appl. **19**, 054047 (2023).

[12] T. M. Fuchs, D. G. Uitenbroek, J. Plugge, N. van Halteren, J.-P. van Soest, A. Vinante, H. Ulbricht, and T. H. Oosterkamp, *Measuring gravity with milligram levitated masses*, Science Advances **10**, eadk2949 (2024).

[13] C. Timberlake, E. Simcox, and H. Ulbricht, *Linear cooling of a levitated micromagnetic cylinder by vibration*, (2023).

[14] A. Bachtold, J. Moser, and M. I. Dykman, *Mesoscopic physics of nanomechanical systems*, Rev. Mod. Phys. **94**, 045005 (2022).

[15] A. Caciagli, R. J. Baars, A. P. Philipse, and B. W. Kuipers, *Exact expression for the magnetic field of a finite cylinder with arbitrary uniform magnetization*, Journal of Magnetism and Magnetic Materials **456**, 423 (2018).

[16] C. Timberlake, G. Gasbarri, A. Vinante, A. Setter, and H. Ulbricht, *Acceleration sensing with magnetically levitated oscillators above a superconductor*, Applied Physics Letters **115**, 224101 (2019).